# Anisotropic Reactive Ion Etching of Silicon Using $SF_6/O_2/CHF_3$ Gas Mixtures

**Rob Legtenberg, Henri Jansen, Meint de Boer, and Miko Elwenspoek**

*MESA Research Institute, University of Twente, 7500 AE Enschede, The Netherlands*

ABSTRACT

Reactive ion etching of silicon in an RF parallel plate system, using $SF_6/O_2/CHF_3$, plasmas has been studied. Etching behavior was found to be a function of loading, the cathode material, and the mask material. Good results with respect to reproducibility and uniformity have been obtained by using silicon as the cathode material and silicon dioxide as the masking material for mask designs where most of the surface is etched. Etch rate, selectivity, anisotropy, and self-bias voltage have been examined as a function of $SF_6$ flow, $O_2$ flow, $CHF_3$ flow, pressure, and the RF power, using response surface methodology, in order to optimize anisotropic etching conditions. The effects of the variables on the measured responses are discussed. The anisotropic etch mechanism is based on ion-enhanced inhibitor etching. $SF_6$ provides the reactive neutral etching species, $O_2$ supplies the inhibitor film forming species, and $SF_6$ and $CHF_3$ generate ion species that suppress the formation of the inhibitor film at horizontal surfaces. Anisotropic etching of high aspect ratio structures with smooth etch surfaces has been achieved. The technique is applied to the fabrication of three-dimensional micromechanical structures.

## Introduction

Dry anisotropic etching of silicon is an important technology for the fabrication of micromechanical devices. Dry etch characteristics are not constrained by crystal planes as in the case of wet anisotropic etching, *e.g.*, by KOH solutions. This has the advantage that not only single-crystalline silicon but also polycrystalline silicon and amorphous silicon can be used for the fabrication of three-dimensional micromechanical structures. Dry etching techniques can be utilized to etch arbitrarily shaped mask designs. This is especially useful for the fabrication of electrostatically driven microactuators that often exhibit complex shapes and require small gap sizes with high aspect ratios.

Dry anisotropic etching of silicon has been achieved with Cl and Br containing gas mixtures like $SF_6$-$CBrF_3$, [1] $SF_6$-$C_2Cl_3F_3$, [2] and $SF_6$-$C_2ClF_5$. [3,4] Also etching of silicon with $SF_6$ at very low temperatures[5] or at very low pressures[6] can be used to produce anisotropic etch profiles. Furthermore $SF_6/O_2$ gas mixtures[7-14] were found to anisotropically etch silicon. The last technique has the advantage of being a fluorine based etch chemistry that can be used in common reactive ion etch systems. However, generally rough etch surfaces are produced that make the process less useful.

In this study the goal was to optimize the anisotropic etching of silicon by $SF_6$-$O_2$ plasmas and produce smooth etch surfaces by response surface methodology, using the etch system described below. This was accomplished by the addition of $CHF_3$ to the $SF_6/O_2$ plasma. The process is applied in the fabrication of micromechanical structures with high aspect ratios.

## Experimental

*Equipment.*—Etching experiments were performed in an Electrotech, Plasmafab 310-340 twin deposition/etch system. The RIE part consists of a parallel-plate system with an RF generator operating at 13.56 MHz and an automatic RF matching network. The pumping system consists of a turbopump in series with a rotary pump. The spacing between the electrodes is fixed at 8.0 cm. The chamber walls consist of aluminum and the powered electrode has a diameter of 19 cm and is covered with a titanium dioxide coated aluminum (styros) plate. The temperature of the lower electrode can be controlled from 10-60°C, by backside heating or cooling, using a temperature controlled oil-bath system. The flow rates of the gases were maintained with standard mass flow controllers. The pressure during processing is monitored with a capacitive manometer and controlled automatically with a throttle valve.

*Initial experiments.—Loading.*—Initial experiments showed that the etch behavior of silicon in $SF_6/O_2$ gas mixtures is loading dependent with regard to macroloading (*i.e.*, the amount of wafers) and with regard to microloading (*i.e.*, with regard to the pattern density on the wafers). This effect has been investigated by several researchers.[15,16] For our purpose we are interested in positive mask pattern designs that are equally distributed over the wafer, and where most of the wafer surface will be etched. The loading was kept constant at one 3 in. wafer per run in our experiments.

*Cathode material.*—The etching behavior is also depending on the cathode material.[15] Three cathode materials; styros, graphite, and silicon have been examined. The graphite and silicon electrode cover the styros electrode that is normally present in the reactor. Styros is a nonconsumable material, in contrast to graphite and silicon, which are etched in fluorine based plasmas. With the styros cathode, the etch rate at the wafer edge was twice as high compared to the etch rate at the center of the wafer. This nonuniformity is a result of gradients in local reactant concentrations and is controlled by the relative etch rates of the wafer *vs.* the cathode material.[15] The uniformity of the etch rate in case of the graphite cathode was measured to be about 20%. The use of the consumable silicon cathode resulted in a uniformity of a few percent across the wafer. In this case the silicon etching rate as well as the selectivity to silicon dioxide were found to be lower than in case of the other cathode materials. Because of the good uniformity, the silicon cathode was used for further experiments.

*Mask material.*—During initial experiments, it was observed that etching is also affected by the mask material. It has been suggested that the mask material may act as a catalyst for $SF_6$ to generate fluorine[19,20] thereby affecting the process conditions. For this reason a noncatalytic mask material is preferred. In our experiments silicon dioxide has been used as the etch mask material.

*$CHF_3$ addition.*—Anisotropic etching with $SF_6/O_2$ plasmas normally produces rough etch surfaces. The silicon etch surfaces sometimes showed a black color as a result of large surface roughness (black silicon). This phenomenon has also been reported by other investigators.[7,9,11] It was found that the addition of $CHF_3$ to the $SF_6/O_2$ plasma produced smooth etch surfaces. Therefore this gas mixture has been used in our experiments.

*Sample preparation.*—In all of the experiments, the samples prepared were 3 in. diam, <100> oriented, p-type (5-10 Ω cm) silicon wafers. A 3000 Å thick $SiO_2$ layer was grown by wet oxidation at 1000°C. This layer was patterned by lithography and RIE using $CHF_3$ gas with a flow of 10 sccm, a process pressure of 20 mTorr, and an RF power of 50 W. The temperature of the oil bath, that controls the temperature of the lower electrode, was set at 25°C. After the etching of the $SiO_2$ layer the resist was stripped by oxygen ashing. Before the etching experiments the etching

**Table I. Nonrandomized experimental design for five normalized parameters.**

| Run no. | $SF_6$ | $O_2$ | $CHF_3$ | p | P |
|---|---|---|---|---|---|
| 1 | −1 | −1 | −1 | −1 | +1 |
| 2 | +1 | −1 | −1 | −1 | −1 |
| 3 | −1 | +1 | −1 | −1 | −1 |
| 4 | +1 | +1 | −1 | −1 | +1 |
| 5 | −1 | −1 | +1 | −1 | −1 |
| 6 | +1 | −1 | +1 | −1 | +1 |
| 7 | −1 | +1 | +1 | −1 | +1 |
| 8 | +1 | +1 | +1 | −1 | −1 |
| 9 | −1 | −1 | −1 | +1 | −1 |
| 10 | +1 | −1 | −1 | +1 | +1 |
| 11 | −1 | +1 | −1 | +1 | +1 |
| 12 | +1 | +1 | −1 | +1 | −1 |
| 13 | −1 | −1 | +1 | +1 | +1 |
| 14 | +1 | −1 | +1 | +1 | −1 |
| 15 | −1 | +1 | +1 | +1 | −1 |
| 16 | +1 | +1 | +1 | +1 | +1 |
| 17 | −2 | 0 | 0 | 0 | 0 |
| 18 | +2 | 0 | 0 | 0 | 0 |
| 19 | 0 | −2 | 0 | 0 | 0 |
| 20 | 0 | +2 | 0 | 0 | 0 |
| 21 | 0 | 0 | −2 | 0 | 0 |
| 22 | 0 | 0 | +2 | 0 | 0 |
| 23 | 0 | 0 | 0 | −2 | 0 |
| 24 | 0 | 0 | 0 | +2 | 0 |
| 25 | 0 | 0 | 0 | 0 | −2 |
| 26 | 0 | 0 | 0 | 0 | +2 |
| 27 | 0 | 0 | 0 | 0 | 0 |
| 28 | 0 | 0 | 0 | 0 | 0 |
| 29 | 0 | 0 | 0 | 0 | 0 |
| 30 | 0 | 0 | 0 | 0 | 0 |
| 31 | 0 | 0 | 0 | 0 | 0 |
| 32 | 0 | 0 | 0 | 0 | 0 |

chamber was manually cleaned with ethanol and by an oxygen plasma cleaning step. Before each experiment the wafer was given an HF dip ($HF:H_2O$ = 1:100) for 1 min to remove the native oxide layer. The gas flows and process pressure were allowed to stabilize for 5 min before etching was performed.

*Experimental design.*—The characteristics of the etch process are explored using a statistical experimental design[21,22] and are modeled empirically by response surface methodology. In general a design should be chosen that will support a full quadratic model, which includes linear terms, two factor interactions, and quadratic terms for curvature. The general form of the full quadratic model is

$$Y = b_0 + \sum_{i=1}^{f} b_i X_i + \sum_{i=1}^{f} b_{ii} X_i^2 + \sum_{i=1}^{f-1} \sum_{j=2}^{f} b_{ij} X_i X_j \qquad [1]$$

where the $X_i$ represent the independent input variables (*i.e.*, process parameters), the $b_i$ are the coefficients for the linear terms, the $b_{ii}$ are the coefficients for the quadratic terms, and the $b_{ij}$ are the coefficients for the cross terms.

For the optimization of the RIE process the $SF_6$ flow, the $O_2$ flow, the $CHF_3$ flow, the pressure, and the RF power have been chosen as the process variables. These process variables have been varied within the limits of our etching system. The temperature of the oil bath that controls the cathode temperature was set at 25°C. No special clamping, or temperature control of the wafer was used. The loading was constant at one 3 in. wafer. A central composite rotatable second order design was used for the experiment. The monitored responses are the self-bias voltage, the silicon etch rate, the uniformity, the etch surface roughness, the selectivity, and the anisotropy. The normalized experimental design information is given in Table I whereas Table II shows the actual parameter settings. The order of performing the experimental trials was randomized to minimize the effect of any systematic error.

**Table II. Variable settings used for the experimental design.**

| Variable | −2 | −1 | 0 | 1 | 2 |
|---|---|---|---|---|---|
| $SF_6$ flow [sccm] | 10 | 20 | 30 | 40 | 50 |
| $O_2$ flow [sccm] | 2 | 6 | 10 | 14 | 18 |
| $CHF_3$ flow [sccm] | 2 | 7 | 12 | 17 | 22 |
| Pressure [mTorr] | 20 | 60 | 100 | 140 | 180 |
| Power [Watt] | 20 | 60 | 100 | 140 | 180 |

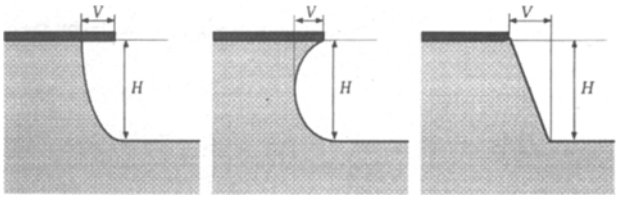


**Fig. 1. Definition of anisotropy.**

*Data acquisition.*—The thickness of the $SiO_2$ layer was measured by ellipsometry before and after the etching process to determine the etch rate of this layer. A correction was made for the HF dip which was measured to remove about 50 Å of the oxide layer before the experiments. After etching, the etch depth of the silicon was measured with a Dektak surface profiler. The result was corrected for the remaining thickness of the oxide layer. The etch depth was measured at the center and at four points at about 1 cm from the edge of the wafer to obtain an indication of the uniformity of the etch process. The selectivity was found from the ratio of the silicon etch depth and the difference in the $SiO_2$ thickness before and after the experiment. To determine the anisotropy, the samples were broken and their cross-section was examined by SEM. Several different etch profiles have been obtained. Depending on the process conditions not only mask undercut, but also outward sloped profiles have been observed. The anisotropy is defined by

$$A = 1 - \frac{V}{H} \qquad [2]$$

where $H$ is the etch depth and $V$ is the maximal undercut of the mask or, in case of outward sloped profiles, the lateral extension of the sidewall as shown in Fig. 1. This definition of the anisotropy does not give information whether the anisotropy is due to mask undercut or to outward sloped profiles. However the expression in Eq. 2 is generally used and therefore preferred for a comparison with results from other workers. A value of 1 represents a perfect vertical sidewall with no mask undercut.

The roughness of the etch surface was only regarded qualitatively by means of the visual reflectivity of the silicon surface after etching, and by examining the etch surface from the cross-sectional SEM photographs.

In our experiments post structures and lines and spacings of 1, 2, and 5 μm have been used to determine the etch rate and anisotropy for etch depth of about 2 μm. At these dimensions no feature size dependent etch effects have been noticed. However, effects like RIE lag and charging, may affect etch results at larger etch depths.[17]

## Results and Discussion

The responses of the factorial design are shown in Table III. The independent input variables in Eq. 1 have been normalized as follows

$$X_i = (\phi_i - \bar{\phi}_i)/\sigma_i \qquad [3]$$

where $X_i$ is the normalized value for the variable setting, $\phi_i$, $\bar{\phi}_i$ is the centerpoint value of that variable, and $\sigma_i$ is the step of the variable that has been used in the factorial design (see Table II).

The responses of the self-bias voltage, the silicon etch rate, the selectivity, and the anisotropy are fitted by the quadratic model (Eq. 1). The regression coefficients $b_i$, $b_{ii}$, $b_{ij}$, and the fit coefficient $R^2$ for the quadratic model are shown in Table IV. Graphical representation of the responses and SEM photographs of sample cross sections are shown in Fig. 2-8. In the graphs all parameters except for the specific parameters being varied are fixed at the center point of the design.

**Table III. Responses of the factorial design. In case of outward sloped etch profiles the anisotropy is marked by an asterisk.**

| Run no. | Bias Voltage [V] | Rate [μm/min] | Selectivity | Anisotropy | Uniformity [%] | Surface |
|---|---|---|---|---|---|---|
| 1 | 477 | 0.430 | 5.9 | 0.590 | 1.0 | smooth |
| 2 | 47 | 0.320 | 13 | 0.690 | 2.4 | smooth |
| 3 | 232 | 0.200 | 4.7 | 0.940* | 2.8 | rough |
| 4 | 339 | 0.670 | 10 | 0.880 | 3.9 | smooth |
| 5 | 224 | 0.200 | 5.2 | 0.810 | 2.0 | smooth |
| 6 | 343 | 0.460 | 5.1 | 0.620 | 3.9 | smooth |
| 7 | 517 | 0.420 | 6.3 | 0.980 | 5.8 | smooth |
| 8 | 72 | 0.310 | 10 | 0.960 | 1.2 | smooth |
| 9 | 31 | 0.120 | 14 | 0.886* | 1.9 | rough |
| 10 | 50 | 0.550 | 11 | 0.560 | 4.2 | smooth |
| 11 | 224 | 0.400 | 6.0 | 0.810* | 1.3 | rough |
| 12 | 27 | 0.055 | 13 | 0.700 | 2.7 | smooth |
| 13 | 154 | 0.350 | 5.6 | 0.640 | 8.1 | smooth |
| 14 | 28 | 0.130 | 30 | 0.460 | 1.9 | smooth |
| 15 | 42 | 0.190 | 12 | 0.886* | 2.7 | rough |
| 16 | 64 | 0.580 | 10 | 0.940 | 4.9 | smooth |
| 17 | 366 | 0.240 | 5.1 | 0.881* | 3.6 | rough |
| 18 | 47 | 0.490 | 12 | 0.690 | 2.3 | smooth |
| 19 | 62 | 0.360 | 6.4 | 0.940 | 7.6 | smooth |
| 20 | 108 | 0.350 | 11 | 0.970* | 1.2 | rough |
| 21 | 58 | 0.360 | 9.3 | 0.938* | 2.2 | rough |
| 22 | 135 | 0.360 | 7.7 | 0.830 | 5.2 | smooth |
| 23 | 448 | 0.360 | 5.9 | 0.730 | 3.8 | smooth |
| 24 | 35 | 0.270 | 20 | 0.844* | 3.7 | rough |
| 25 | 23 | 0.007 | 6.8 | 0.900 | 3.3 | smooth |
| 26 | 356 | 0.600 | 7.2 | 0.660 | 3.5 | smooth |
| 27 | 88 | 0.450 | 9.7 | 0.970 | 5.5 | smooth |
| 28 | 85 | 0.440 | 10 | 0.940 | 6.3 | smooth |
| 29 | 86 | 0.430 | 9.2 | 0.950 | 3.8 | smooth |
| 30 | 84 | 0.450 | 10 | 0.970 | 2.3 | smooth |
| 31 | 87 | 0.430 | 8.9 | 0.970 | 3.7 | smooth |
| 32 | 85 | 0.430 | 9.4 | 0.960 | 3.9 | smooth |

*Etch rate.*—In Fig. 2 the effect of the $SF_6$ and $O_2$ flow, and the effect of the pressure and RF power, on the etch rate of silicon are shown. The silicon etch rate shows a quadratic dependency on the $SF_6$ flow, the $O_2$ flow, the process pressure, and the RF power. The rate is independent of the $CHF_3$ flow. The accuracy of the model is indicated by the squared multiple $R^2$ which is 0.99 and represents a good fit.

To understand the etch behavior, some background of the etch mechanism is needed. It is well known that plasma etching of silicon with fluorinated compounds is primarily due to free fluorine.[23] The dissociation of $SF_6$ is assumed to involve electron impact dissociation reactions of the form

$$e + SF_{x_g} \rightarrow SF_{x-1_g} + F_g + e \ (x = 3 - 6) \quad [4]$$

The etching of silicon occurs by a reaction with F atoms. The overall stoichiometry of etching by atomic F is[24]

**Table IV. Fitted coefficients of the quadratic model for the responses. The *s* value at the bottom of each column is an estimate of the standard deviation for that response. The $R^2$ index indicates the agreement between model and data. A value of 1.00 denotes an ideal fit.**

| Coef. | Rate | Selectivity | Anisotropy | DCB |
|---|---|---|---|---|
| b0 | 0.434 | 9.34 | 0.969 | 87 |
| b1 | 0.052 | 2.34 | −0.066 | −65 |
| b2 | 0.010 | −0.36 | 0.079 | 11 |
| b3 | 0.004 | −0.14 | 0.004 | 7 |
| b4 | −0.043 | 2.90 | 0.008 | −102 |
| b5 | 0.147 | −1.72 | −0.043 | 89 |
| b11 | −0.014 | −0.05 | −0.040 | 29 |
| b22 | −0.017 | −0.01 | −0.013 | −1 |
| b33 | −0.016 | −0.06 | −0.023 | 2 |
| b44 | −0.027 | 1.05 | −0.035 | 38 |
| b55 | −0.030 | −0.44 | −0.056 | 25 |
| b12 | 0.003 | −0.90 | 0.029 | −6 |
| b13 | −0.008 | 0.60 | 0.004 | 4 |
| b14 | −0.016 | 0.65 | −0.039 | 23 |
| b15 | 0.035 | −1.11 | 0.058 | −14 |
| b23 | 0.028 | 0.16 | 0.054 | −17 |
| b24 | −0.007 | −1.34 | −0.016 | 2 |
| b25 | 0.018 | 1.70 | 0.035 | 5 |
| b34 | 0.022 | 1.29 | −0.019 | 7 |
| b35 | −0.023 | −1.15 | 0.028 | −3 |
| b45 | 0.027 | −1.93 | 0.008 | −46 |
| s | 0.01 | 0.5 | 0.01 | 1.5 |
| $R^2$ | 0.99 | 0.90 | 0.95 | 0.99 |

$$Si + 4F \rightarrow SiF_4 \quad [5]$$

The etch rate $R_{Si}$ can be written as

$$R_{Si} = k\beta_{Si}n_F \quad [6]$$

where $k$ is a proportionality constant, $\beta_{Si}$ is the reaction probability of fluorine at the surface and $n_F$ is the density of

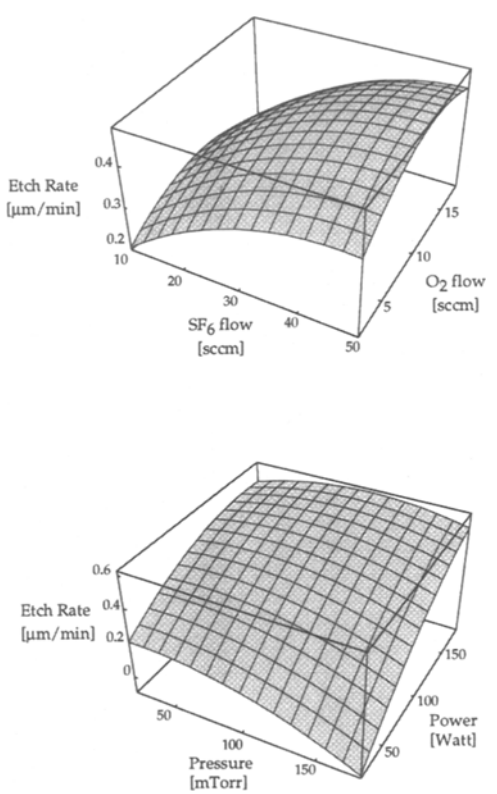


**Fig. 2. Surface plots showing the silicon etch rate as a function of the $SF_6$ and $O_2$ flow, and as a function of the process pressure and the RF power. All parameters except for the specific parameters being varied are fixed at the center point of the design.**

fluorine atoms. Higher $SF_6$ flows will increase the fluorine concentration in the gas mixture, resulting in higher etch rates. At high flows, the fluorine concentration can decrease due to higher convective losses (see section on total flow rate) and the etch rate will start to decrease.

The influence of oxygen addition to $SF_6$ plasmas has been investigated by several authors.[11-14,25-27] With an $SF_6$-$O_2$ mixture in the absence of silicon, the final reaction products are $F_2$, $SOF_4$, and $SO_2F_2$. When Si is etched, $SiF_4$ is the only stable silicon-containing etch product and $SOF_2$ is formed in oxygen-poor mixtures. It was found that oxygen additions drastically increase the conversion of the feed gas, evidently by reacting with fluorosulfur radicals and thus preventing their recombination with fluorine to reform $SF_6$.[12]

$$SF_x + F \rightarrow SF_{x+1} \; (x = 5 - 1) \qquad [7]$$

This leads to a net increase of F atoms. As the feed is made more $O_2$ rich, $SO_2F_2$ increases with respect to $SOF_4$ while the F-atom concentration first increases, reaches a maximum, and then decreases. These results closely parallel analogous trends in the carbon-based $CF_4$-$O_2$ system.[25]

When silicon is exposed to the discharge, a significant change in the product composition is observed. $SOF_2$ is formed in oxygen-poor mixtures, $SiF_4$ appears, and the concentration of molecular fluorine is depressed.[13] As the quantity of oxygen is increased, the etch rate goes through a maximum and subsequently decreases.

In the presence of oxygen, oxygen species compete with F for active surface sites. This has been explained by a quantitative model which takes oxygen adsorption into account to relate the etch rate to the fluorine concentration for silicon and $SiO_2$ etching in $CF_4$-$O_2$ plasmas.[24] The decrease of the reaction probability is found to be

$$\beta' = \frac{\beta}{1 + C n_O / n_F} \qquad [8]$$

where $\beta'$ is the reaction probability in the presence of oxygen, $n_O$ is the density of oxygen atoms, and $C$ is a constant. Maneschijn[28] showed that this model also represents the data for $SF_6$-$O_2$ gas mixtures quite well.

Thus at higher $O_2$ flows the etch rate will be depressed as a result of the competition of oxygen atoms with fluorine atoms for chemisorption on the silicon surface.

As was pointed out by Tzeng[11] increasing the RF power leads to a significant increase of the atomic fluorine concentration while the oxygen concentration increases only slightly. This explains the increased silicon etching rate with increasing RF power.

At low RF power the etch rate decreases with increasing pressure, while at high RF power the etch rate first increases, reaches a maximum, and finally decreases with increasing pressure. These results agree with the experiments of Kopalidis.[12] By measuring the effect of pressure on the discharge composition of $SF_6$-$O_2$ plasmas they found that the main effect of increasing pressure is to enhance the oxyfluoride production rates, thus reducing the recombination reactions. In accordance with our results, the self-bias was found to decrease strongly with increasing pressure. Assuming that ion bombardment contributes significantly to the overall etching rate (the synergistic effect of ion bombardment and chemical etching), the decrease in the etch rate with increasing pressure can be explained by the decrease in ion bombardment at higher pressures.

At high RF power the initial increase of the etch rate with increasing pressure may be the result of an increasing $F$ concentration and ion density that leads to a larger ion flux toward the substrate.

*Selectivity.*—The selectivity is linearly increasing with the $SF_6$ flow, and linearly decreases with the $O_2$ flow and the RF power and only slightly decreases with increasing $CHF_3$ flow. It shows a quadratic dependency on the pressure. Surface plots showing the selectivity as a function of the $SF_6$ and the $O_2$ flow, and as a function of the process pressure and the RF power are shown in Fig. 3. The $R^2$ index indicates a good model fit.

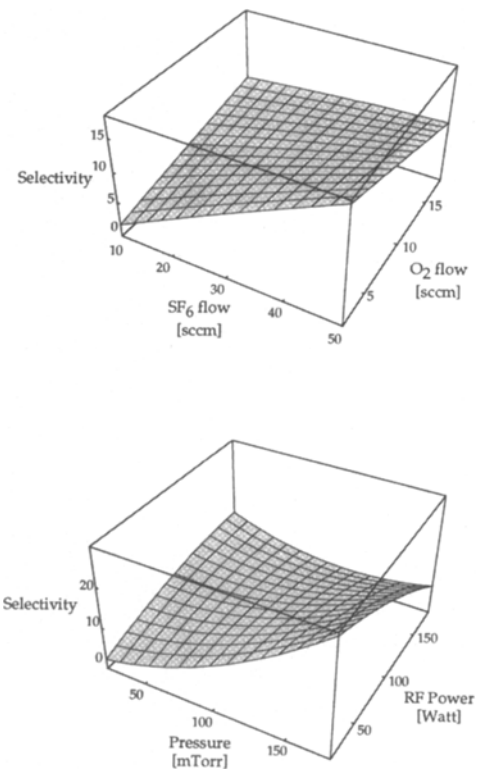


**Fig. 3. Surface plots showing the selectivity as a function of the $SF_6$ and the $O_2$ flow, and as a function of the process pressure and the RF power.**

The selectivity is the quotient of the etch rates of silicon and silicon dioxide. The effect of the process parameters on the silicon etch rate have been discussed. The etch rate of

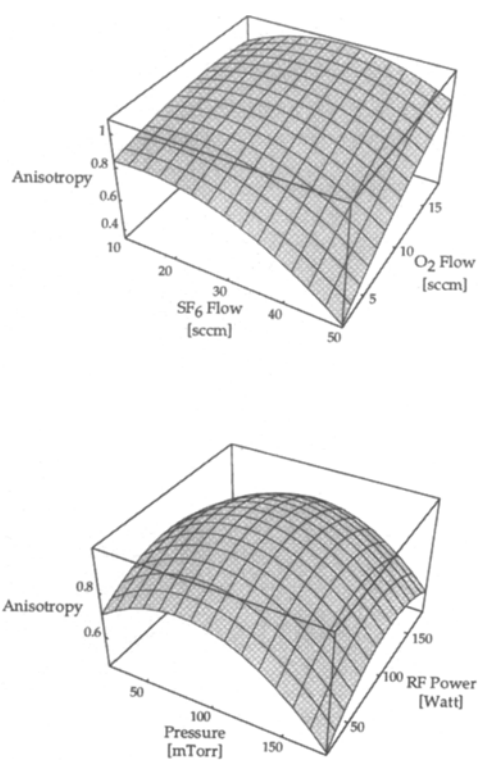


**Fig. 4. Surface plots showing the anisotropy as a function of the $SF_6$ and $O_2$ flow, and as a function of the process pressure and the RF power.**

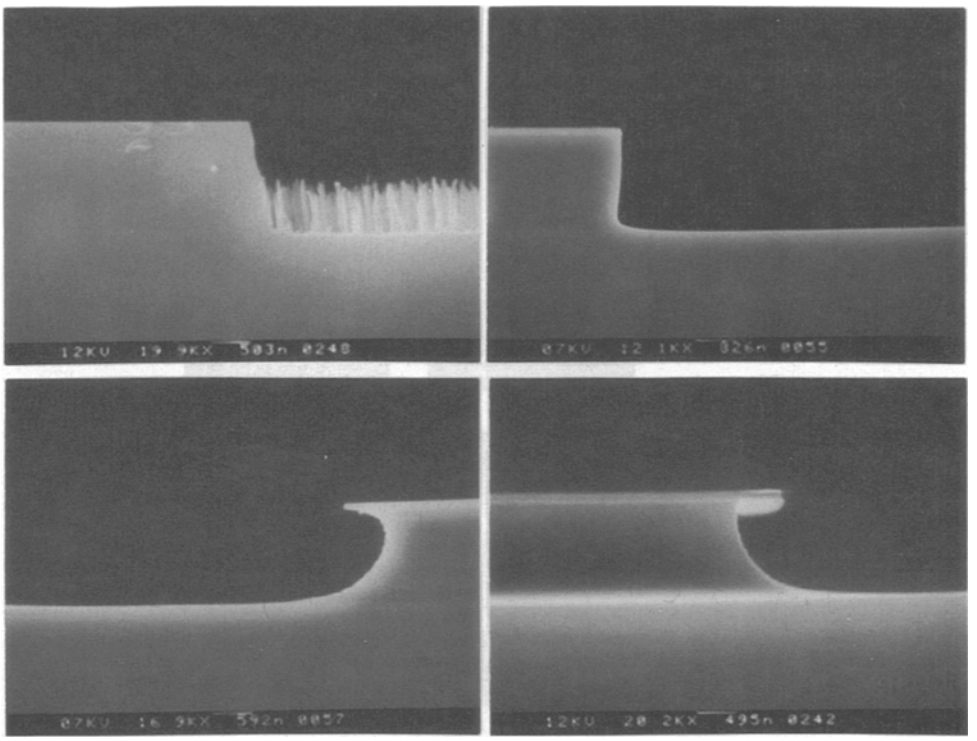

Fig. 5. Sidewall profiles obtained under different process conditions. The parameter settings are shown in Tables I and II for: (a, top left) fact. nr. 24, (b, top right) fact. nr. 27, (c, bottom left) fact. nr. 13, and (d, bottom right) fact. nr. 6.

$SiO_2$ is to a large extent due to direct etching by reactive ions. It was reported that the etch rate of $SiO_2$ in a $CHF_3$-$O_2$ plasma was found to follow the ion density and to be fairly independent of the plasma chemistry under most experimental conditions.[29] Ion bombardment increases with increasing RF power and with decreasing pressure. This results in a decrease of the $SiO_2$ etch rate with increasing RF power and an increase of the $SiO_2$ etch rate with increasing pressure. Assuming that the $SiO_2$ etch rate in this process is also fairly independent of the plasma chemistry, this leads to an increase of the selectivity with increasing $SF_6$ flow and increasing pressure (more chemical etching) and a decrease of the selectivity with increasing RF power and $O_2$ flow and $CHF_3$ flow (more physical etching).

*Anisotropy.*—Responses of the anisotropy are shown in Fig. 4. The anisotropy shows a linear increase with the $O_2$ flow. It is quadratically dependent on the process pressure, the RF power, and the $SF_6$ flow. Furthermore, the anisotropy shows a weak quadratic dependency on the $CHF_3$ flow. Again the fit between the data and the model is good.

In Fig. 5 a selection of the sidewall profiles, that have been obtained in our experiments, is shown. These photographs clearly demonstrate that it is difficult to obtain a straightforward definition of the anisotropy. Depending on process conditions profiles may vary from isotropic to outward sloped profiles. Note that at high pressures and high $O_2$ flows the value of the anisotropy, as defined before, may be lower because of outward sloped etch profiles.

Auger electron spectroscopy (AES) data, taken within 15 min after the etch process, from the sidewall and bottom etch surfaces of a center point run is shown in Fig. 6. On both surfaces about equal amounts of sulfur and carbon were detected. Sulfur most likely is a product of the $SF_6$ gas and carbon may result from the $CHF_3$ gas or from organic contamination. The presence of fluorine was not observed. However, this may be due to electron stimulated desorption of fluorine atoms as a result of the measurement. On both surfaces oxygen is present. The amount of oxygen on the sidewall surface is much higher than the amount of oxygen on the bottom surface. This clearly indicates a sidewall passivation effect by oxygen species, as proposed by Zhang.[14] On the horizontal silicon surfaces, adsorption of oxygen residue can be readily attacked through the physical bombardment of active ion species like $SF_x^+$ and $CF_x^+$. While on the vertical Si surfaces (sidewalls), the removal of sidewall material is not significant because of the less directional kinetic energy in this orientation. These results are in agreement with other investigations.[7,30,31]

Surface and interfacial residue films formed on polycrystalline silicon and silicon dioxide by reactive ion etching with $SF_6$-10% $O_2$ at 100 mTorr have been investigated using x-ray photoemission spectroscopy.[30] Composition and chemistry at the surface were found to be variations of $SiO_xF_y$. The thickness varied from 7-13 Å with decreasing etch rate.

Silicon surfaces etched in $CF_4$-$O_2$ plasma have been characterized with the use of *in situ* x-ray photoemission spectroscopy.[31] An $SiF_xO_y$ layer on elemental silicon was found to be formed under all conditions. For oxygen percentages greater than 5% in the feed gas, the oxygen content of the film and the film thickness increased, whereas the fluorine content of the film decreased.

These observations may explain the increase of the anisotropy with increasing $O_2$ flow and the decrease of the anisotropy with increasing $SF_6$ flow by affecting the formation of the sidewall passivation layer. At high $O_2$ flows and low $SF_6$ flows, profiles are positively tapered (outward sloped) and the anisotropy shows an initial increase with the $SF_6$ flow. In this region, the formation of the passivation layer is very pronounced and outward sloped etch profiles are obtained that may be the result of an orientation dependent etch rate on the passivation layer. Increasing the $SF_6$ flow at high $O_2$ flow, increases the F concentration, thereby reducing the formation of the passivation layer on outward sloped profiles which leads to a more vertical etch profile that has a higher anisotropy.

Increasing the pressure has been found to increase the atomic fluorine concentration and decrease the ion bombardment.[12] Both effects lead to a reduction of the anisotropy, in agreement with our results at high pressures. However, at low pressures the anisotropy increases with increasing pressure till it reaches a maximum. This may be explained by a low silicon surface coverage by oxygen atoms. The surface coverage is a function of the pressure and increases with increasing pressure. Apparently the oxygen concentration at low pressures is too small to result in a surface coverage that is high enough to form a stable passivation layer. The RF power gives an initial increase,

reaches a maximum, and then results in a decrease of the anisotropy with increasing RF power. Increasing the RF power increases the F concentration as well as the ion bombardment on the horizontal surface. At low RF power it seems that the effect of the increase in ion bombardment is stronger than the effect of the increasing F concentration, giving a net increase in the anisotropy. At higher RF power the increase in the F concentration probably becomes dominant and reduces the formation of the passivation layer. This leads to a decrease in the anisotropy with increasing RF power.

Adding $CHF_3$ to the $SF_6$-$O_2$ plasma may influence the O to F concentration. In $CHF_3$-$O_2$ plasmas the major reaction products are $CF_x$ species, CO, $CO_2$, and $COF_2$.[29] These reactions will lower the O atom concentration. Since the selectivity (*i.e.*, the $SiO_2$ etch rate) is only slightly affected by the $CHF_3$ addition it is suggested that the formation of the passivation layer is suppressed by an additional competition of oxygen with $CF_x$ species on the surface. This effect is assumed to be more pronounced at the horizontal surfaces because the etch mechanism of silicon oxide, by $CF_x$ species, is ion enhanced where ions are the main reactants in the etch reaction.[29] For high $CHF_3$ flows the reduction of the O atom concentration and passivation layer formation eventually results in more isotropic etching profiles (see Fig. 8).

*Total gas flow.*—It should be noted that the total gas flow in the experiments is not constant and changes, depending on the $SF_6$, $O_2$, and $CHF_3$ gas flow settings, from a minimum value of 32 sccm to a maximum value of 72 sccm. As a result, the residence time of the gases is not constant. Longer residence times will lead to a higher conversion of the etch gases into lower molecular weight products. The etch rate dependency as a function of the total flow rate for $SF_6/O_2$ gas mixtures has been studied by Tandon and Kopalidis.[8,32] At low pressures, an increase in total flow rate is accompanied by an increase in the dissociation of $SF_x$ molecules and radicals and the etch rate is limited by the supply of fluorine atoms while at high flow rate the etch rate decreases due to convective losses. At high pressure and low flow rate, etchant production is at its maximum and increasing flow rates causes the fluorine concentration to decrease due to higher convective losses (active species are pumped away before they have an opportunity to react).

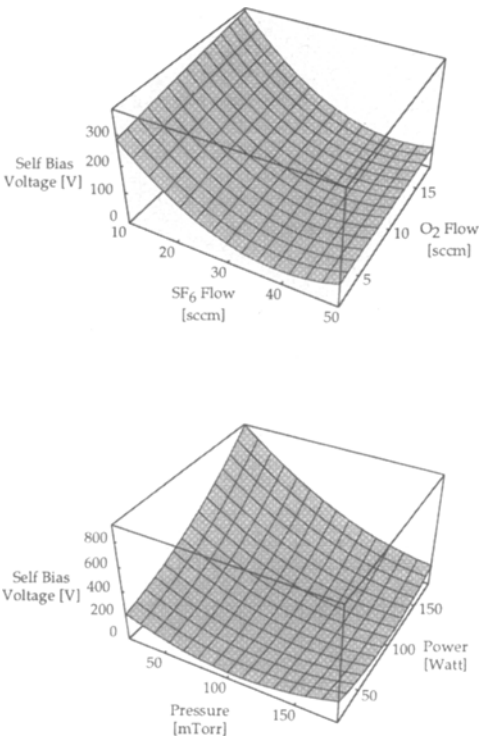


**Fig. 7. Surface plots showing the bias voltage as a function of the $SF_6$ and the $O_2$ flow, and as a function of the process pressure and the RF power.**

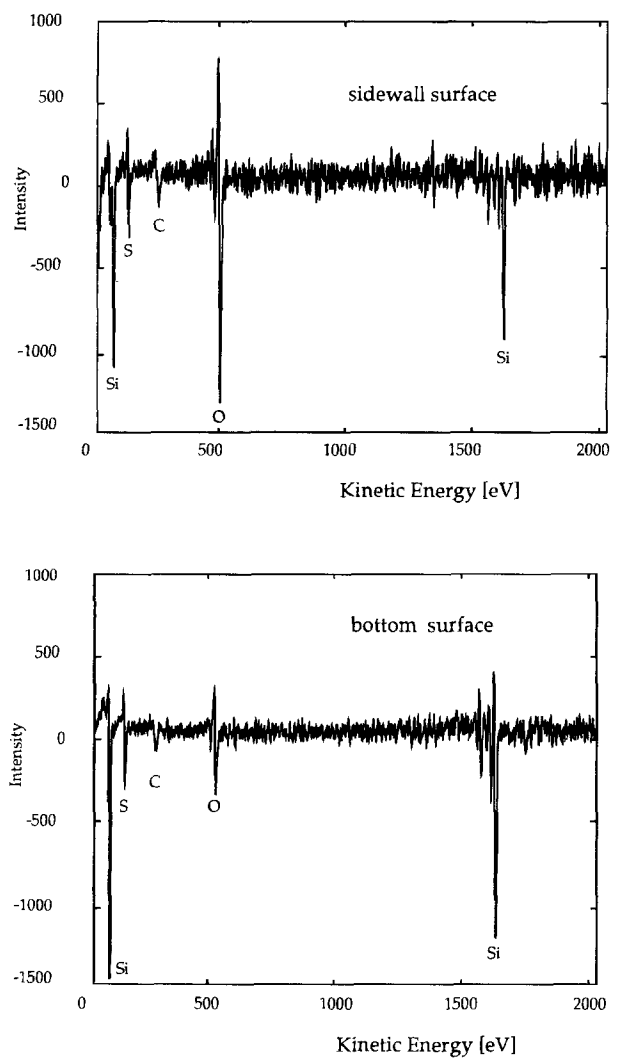


**Fig. 6. AES data of the sidewall and bottom etch surface after etching of a center point run.**

*Uniformity.*—As shown in Table IV the uniformity does not show a large variation when the parameter settings are changed. Only a few points per wafer have been used to determine the uniformity leading to a relatively large standard error. The average uniformity of the etch rate is 3.5% with a standard deviation of 1.4%. A small increase is observed for high $SF_6$ flows and high pressures. The uniformity is mainly a function of loading and cathode material as discussed in the section on initial experiments.

*Self-bias voltage.*—The bias voltage is quadratically dependent on the $SF_6$ flow, the RF power and the pressure. It increases linearly with the $O_2$ flow and the $CHF_3$ flow. The model fit of the experimental values is very good as indicated by the $R^2$ index which equals 0.99. The results are presented graphically in Fig. 7.

$SF_6$ is used as a gaseous insulator because of its electronegativity. Increasing the $SF_6$ flow makes the discharge more electronegative due to a lower ratio of electrons to positive ions and the self-bias voltage decreases.

The decrease of the dc bias voltage with pressure is a result of a decrease in the electron energy as the pressure is increased.[12] The increase of the dc bias with increasing $O_2$ flow and $CHF_3$ flow, is a consequence of a shift of the electron energy distribution to higher values.[12]

*Etch surface roughness.*—It was observed that the etch surface roughness showed a correlation to wafer cleanli-

ness. A cleaning step, followed by an HF dip, was sufficient to reduce the etch surface roughness in this case, indicating that etch residue from previous steps or native oxide could be responsible for this effect. In spite of these precautions rough etch surfaces have been observed after the etching process and were found to be a function of the etch parameters. This indicates that rough etch surfaces are also generated by the etching process itself. At high pressures and high $O_2$ flows, in the anisotropic etching regime, the etch surface roughness increases. The addition of $CHF_3$ to an $SF_6/O_2$ gas mixture improves the etch surface quality, as shown in Fig. 8. When no $CHF_3$ is added, the etch surface roughness, in the anisotropic etch regime, is high as a result

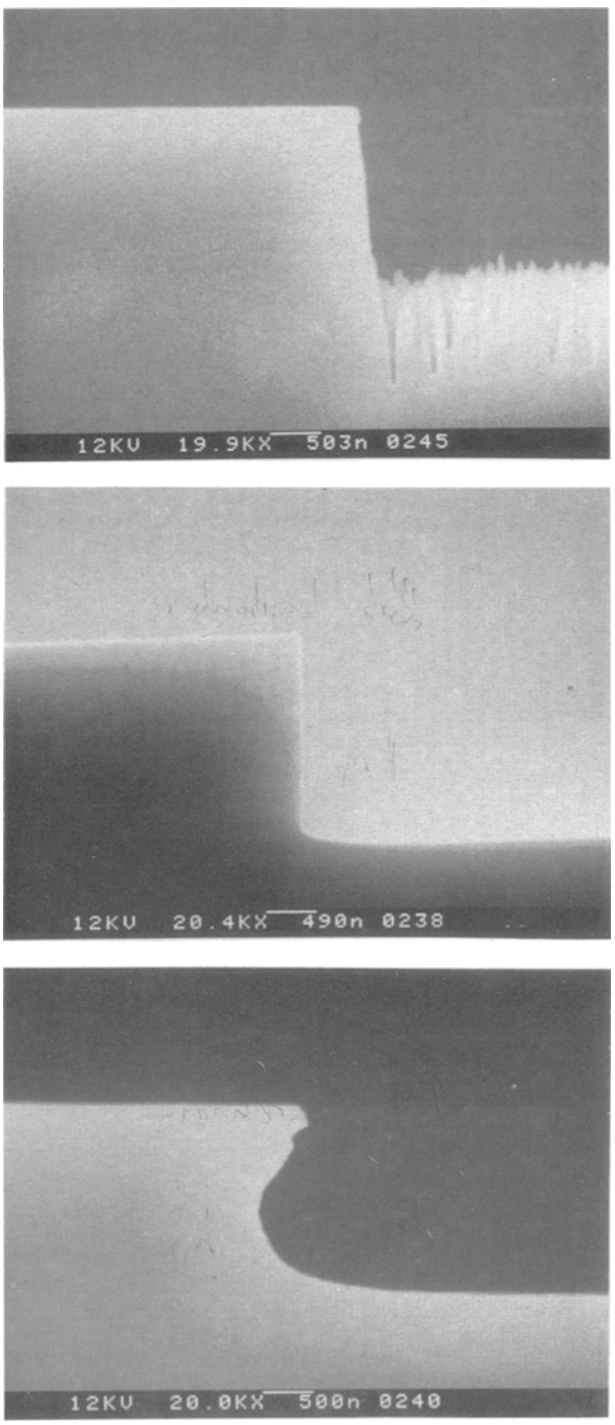


**Fig. 8. SEM photographs showing the influence of the $CHF_3$ addition with respect to the surface roughness and etch profile. All parameter settings except for the $CHF_3$ flow are set at the center point, (a, top) 2 sccm $CHF_3$; (b, middle) 12 sccm $CHF_3$; (c, bottom) 22 sccm $CHF_3$.**

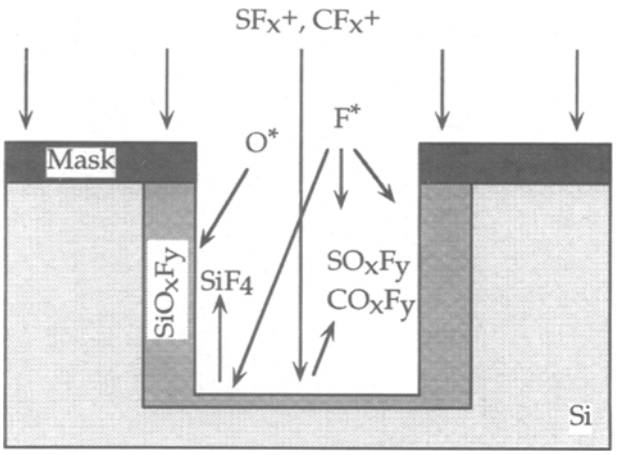


**Fig. 9. Schematic view of the $SF_6$, $O_2$, $CHF_3$ etch process.**

of "micrograss." The addition of $CHF_3$ results in smooth surfaces, only slightly affecting the anisotropy. At high $CHF_3$ flows, the anisotropy will be low and more isotropic etching is obtained.

It is suggested that surface roughness is the result of silicon oxide micromasking. It has been shown that during etching in $SF_6$ plasmas, large amounts of Si particles are generated.[33] When oxygen is added to $SF_6$ plasmas these particles may also contain silicon oxide. Redeposition of these particles on the etch surfaces results in micromasking leading to the development of surface roughness (micrograss) in case of anisotropic etching. Another possibility is that the surface roughness results from variations in thickness of the oxyfluoride layer on the horizontal silicon surfaces. The presence of $CF_x$ species in the plasma may suppress the formation and/or oxidation of the particles that are generated by the plasma or reduce their masking effect and suppresses the formation of the passivation layer on the horizontal surface by chemical and physical attack. Note that $CF_x$ species may not only be produced by the etch gas but also by photoresist or reactor components like a graphite cathode.

In summary it can be concluded that the anisotropic etch mechanism is based upon an ion-enhanced inhibitor etching process. This mechanism requires three ingredients: 1—reactive neutral species, 2—inhibitor film forming species, and 3—vertical ion flux to the substrate to prevent growth or etch the inhibitor film at the horizontal surfaces. These mechanisms can be more or less controlled independently by the three etch gases. $SF_6$ produces the F radicals for the chemical etching of the silicon. $O_2$ creates the O radicals to passivate the silicon surface by silicon oxide species. $CHF_3$ produces $CF_x$ ions that, in addition to $SF_x$ ions, suppress the formation of the passivation layer at horizontal surfaces. The etch process is schematically shown in Fig. 9.

## Applications and Other Mask Materials

The process parameters optimized for high anisotropy are very useful for the fabrication of deep trenches and micromechanical structures. The optimized process parameter settings result in an anisotropy of 0.98, an etch rate of 0.5 μm/min, a selectivity with $SiO_2$ of 10, and a smooth etch surface. Not only monocrystalline silicon but also LPCVD polysilicon and sputtered silicon films have been used to fabricate micromechanical structures. In Fig. 10 and 11 SEM photographs are shown that clearly demonstrate the usefulness of the RIE process for high aspect ratio structures. The selectivity of the silicon dioxide mask limits the etch depth. This problem can be solved by using metal etch masks. For instance with a chromium etch mask very high selectivities (>500) have been obtained, whereas etch characteristics are only slightly affected. Applications of this etch process, with respect to deep trench etching and other mask materials, have been presented elsewhere.[34,35]

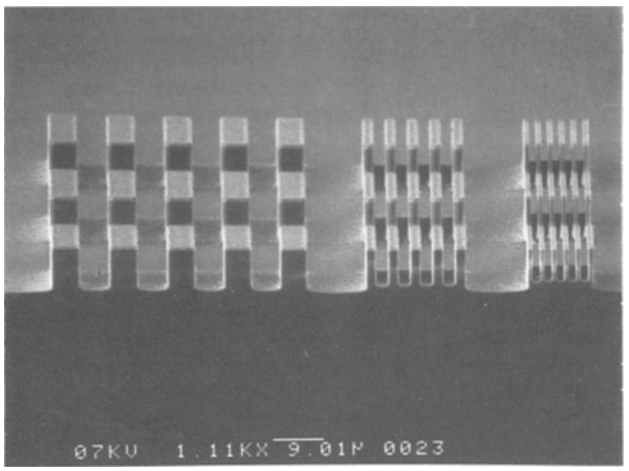


**Fig. 10. SEM photograph showing 1, 2, and 5 μm lines and spacings etched to a depth of about 10 μm. For the 1 and 2 μm structures the effect of RIE lag is clearly visible.**

## Conclusions

Reactive ion etching using $SF_6$, $O_2$, and $CHF_3$ gas mixtures for the anisotropic etching of silicon has been investigated. The etching behavior was found to be affected by loading, the mask material, and the cathode material. Reproducible and uniform results have been obtained using a silicon cathode and a silicon dioxide mask. Surface response methodology was used to characterize etch rate, mask selectivity, bias voltage, and anisotropy as a function of the RF power, the process pressure, the $SF_6$ flow, the $O_2$ flow, and the $CHF_3$ flow in order to optimize anisotropic etching conditions. The effect of several variables on the measured responses has been discussed. The addition of $CHF_3$ can be used to produce smooth etch surfaces in the anisotropic regime and is useful for a fine tuning of the anisotropy.

AES measurements indicate that anisotropic etching results from sidewall passivation by silicon oxide species. The anisotropic etch mechanism in $SF_6$, $O_2$, $CHF_3$ plasmas is based on ion-enhanced inhibitor etching. $SF_6$ provides the reactive neutral etching species in the form of F atoms. $O_2$ supplies the inhibitor film forming species that passivate the surface with an $SiO_xF_y$ layer. $SF_6$ and $CHF_3$ generate ion species, $SF_x^+$ and $CF_x^+$, respectively, that suppress the formation the inhibitor film at horizontal surfaces.

The fabrication of structures with aspect ratios of about 10 has been demonstrated. The process is applied to deep trench etching and fabrication of high aspect ratio structures used in micromachining.

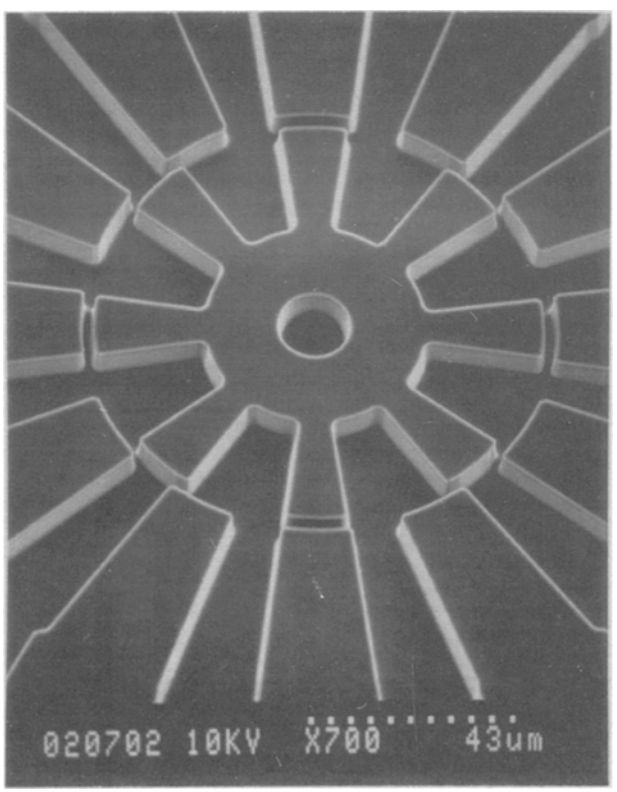


**Fig. 11. SEM photograph of a stator-rotor structure of an electrostatic micromotor. Diameter of the rotor is 100 μm, etch depth is 13 μm, and the rotor-stator gap spacing is 2 μm.**

## Acknowledgments

The authors like to thank Bert Otter and Mark Smithers for doing the SEM work. Also they thank Albert van de Berg for the Auger measurements. This research is part of the program of the Dutch Foundation for Fundamental Research on Matter (FOM) and is sponsored by the Dutch Technology Foundation (STW).

Manuscript submitted May 20, 1994; revised manuscript received March 7, 1995.

*The University of Twente assisted in meeting the publication costs of this article.*

REFERENCES

1. A. M. Krings, K. Eden, and H. Beneking, *Microelectron. Eng.*, **6,** 553 (1987).
2. V. A. Yunkin, D. Fischer, and E. Voges, *ibid.*, **23,** 373 (1994).
3. C. Linder, T. Tschan, and N. F. de Rooy, in *Proceedings of the 6th International Conference on Solid-State Sensors and Actuators (Transducers '91),* p. 524 (1991).
4. J. P. McVittie and C. Gonzalez, Abstract 405, p. 584, The Electrochemical Society Extended Abstracts, New Orleans, LA, Oct. 7-12, 1989.
5. A. J. Watts and W. J. Varhue, *J. Vac. Sci. Technol. A,* **10,** 1313 (1992).
6. C. Pomot, B. Mahi, B. Petit, Y. Arnal, and J. Pelletier, *ibid.*, **4,** 1 (1986).
7. T. Syau, B. J. Baliga, and R. W. Hamaker, *This Journal,* **138,** 3076 (1991).
8. U. S. Tandon and B. P. Pant, *Vacuum,* **42,** 837 (1991).
9. R. Pinto, K. V. Ramanathan, and R. S. Babu, *This Journal,* **134,** 165 (1987).
10. C. P. D'Ernic, K. K. Chan, and J. Blum, *J. Vac. Sci. Technol. B,* **10,** 1105 (1983).
11. Y. Tzeng and T. H. Lin, *This Journal,* **134,** 2304 (1987).
12. P. M. Kopalidis and J. Jorne, *ibid.*, **139,** 839 (1992).
13. R. d'Agostino and D. L. Flamm, *J. Appl. Phys.*, **52,** 162 (1981).
14. M. Zhang, J. Z. Li, I. Adesida, and E. D. Wolf, *J. Vac. Sci. Technol. B,* **1,** 1037 (1983).
15. A. G. Nagy, *This Journal,* **131,** 1871 (1984).
16. C. J. Mogab, *ibid.*, **124,** 1262 (1977).
17. R. A. Gotscho and C. W. Jurgensen, *J. Vac. Sci. Technol. B,* **10,** 2133 (1992).
18. R. W. Light and H. B. Bell, *This Journal,* **130,** 1567 (1983).
19. G. W. Grynkewich, T. H. Fedynyshyn, and R. H. Dumas, *J. Vac. Sci. Technol. B,* **8,** 5 (1990).
20. T. H. Fedynyshyn, G. W. Grynkewich, and Tso-Ping Ma, *This Journal,* **134,** 2580 (1987).
21. W. G. Cochran and G. M. Cox, *Experimental Designs,* 2nd ed., John Wiley & Sons, Inc. (1964).
22. G. E. P. Box, W. G. Hunter, and J. S. Hunter, *Statistics for Experimentors,* John Wiley & Sons, Inc.
23. Y. Lii and J. Jorné, *This Journal,* **137,** 3633 (1990).
24. C. J. Mogab, A. C. Adams, and D. L. Flamm, *J. Appl. Phys.*, **49,** 3796 (1978).
25. K. R. Ryan, *Plasma Chemistry and Plasma Processing,* **9,** 483 (1989).
26. K. R. Ryan and I. C. Plum, *ibid.*, **10,** 207 (1990).
27. W. W. Brandt and T. Honda, *J. Appl. Phys.*, **60,** 1595 (1986).
28. A. Maneschijn, Ph.D. dissertation, Technical University of Delft, The Netherlands (1991).

29. Ch. Steinbrüchel, H. W. Lehmann, and K. Frick, *This Journal,* **132,** 180 (1985).
30. J. H. Thomas and B. Singh, J. *Vac. Sci. Technol. A,* **10,** 3039 (1992).
31. G. S. Oehrlein, S. W. Robey, and J. L. Lindström, *Appl. Phys. Lett.,* **52,** 1170 (1988).
32. P. M. Kopalidis and J. Jorné, *ibid.,* **140,** 3037 (1993).
33. M. M. Smadi, G. Y. Kong, R. N. Carlile, and S. E. Beck, *ibid.,* **139,** 3356 (1992).
34. H. Jansen, M. de Boer, R. Legtenberg, and M. Elwenspoek, in *Proceedings of Micro Mechanics Europe (MME '94),* p. 60, Pisa, Italy, September 5-6 (1994).
35. H. Janssen, M. de Boer, J. Burger, R. Legtenberg, and M. Elwenspoek, in *Proceedings of Micro and Nano Engineering (MNE),* pp. 475-480, Switzerland, September 26-29 (1994).

# Effects of Drying Methods and Wettability of Silicon on the Formation of Water Marks in Semiconductor Processing

**Jin-Goo Park*,[a] and Michael F. Pas*,[b]**

[a]*Department of Metallurgy and Materials Engineering, Hanyang University, Ansan, 425-791, Korea*
[b]*Texas Instruments Incorporated, Dallas, Texas 75243*

ABSTRACT

In-line observation and classification of water marks after the drying process was investigated with regard to the wettability of wafers and the drying methods applied. The formation of water marks was observed with a KLA wafer inspection system and a particle scanner on different hydrophilic and hydrophobic wafers with and without patterns. The wafers were spun and IPA vapor dried as a function of the air exposure time. The hydrophilic wafers did not create any water marks with either spin or vapor dries. The air exposure time and dry method are much more sensitive with the hydrophobic surfaces in creating water marks. The spin dry of hydrophobic wafers created a large quantity of water marks independent of the air exposure time. Homogeneously hydrophilic or hydrophobic wafers with and without patterns did not create any water marks following the vapor drying of wafers. However, the patterned wafers with both hydrophobic and hydrophilic sites created water marks even in IPA vapor dry. This indicates that the wettability and drying method of the wafer play an important role in creating water marks in semiconductor wet processes.

## Introduction

Contamination such as particles, heavy metals, and organic residues have been well recognized during semiconductor processing. For the removal of these contaminants, wet processes are still dominant during semiconductor fabrication. In the aqueous processing of silicon wafers, drying after rinsing is a critical step and must be accomplished by the physical removal of water from wafer surfaces. The most commonly practiced drying process is spin rinse (SRD) or spin dry (SD). It has been suggested that this method recontaminates the wafer surface with particles and aerosols caused by the mechanical motion of dryer itself.[1] Another drying method is solvent vapor dry (VD), typically using IPA (isopropyl alcohol). This method uses the lower boiling temperature and surface tension of IPA, compared to water, in a closed chamber. Mishima *et al.*[2] found that the water content in IPA, the temperature distribution of IPA in the vapor dryer, and the velocity of IPA affect the cleanliness of surfaces after IPA drying. They determined such optimum conditions for IPA vapor drying to be water content in IPA of less than 1000 ppm, IPA temperature at the wafers of 82°C, and an IPA velocity of 5.0 cm/s. These conditions resulted in the cleanest surfaces during IPA drying.

Hydrophobicity/hydrophilicity of a silicon wafer surface is one of the most important parameters in understanding the source of microcontamination. Oxide-coated and RCA cleaned wafer surfaces are hydrophilic and HF etched surfaces are hydrophobic due to the passivation by hydrogen termination.[3] Hydrophobic surfaces are characterized by large contact angles of water, often in the range 40-110° and low heats of immersion in water, 6-90 dyn/cm. [4] Static contact angles have been measured on HF etched silicon wafers.[5,6] Using methanol/water solutions, Gould and Irene[5] determined a value of critical surface tension ($\gamma_c$), of 27 dyn/cm for Si from static contact angle measurements. This low value of $\gamma_c$ was attributed to the presence of hydrogen and fluorine species on the HF etched Si surface. William and Goodman[6] measured the contact angle of water on silicon surfaces covered with oxide layers of different thicknesses. They found HF-etched silicon to be hydrophobic ($\theta \approx 90°$) and oxides thicker than 30 Å to be hydrophilic ($\theta \approx 0°$). Contact angles were a function of the oxide thickness. The contact angle measurement method is inexpensive and rapid in characterizing the solid surface even though the surface chemistry information is ambiguous.

The HF-last process is most attractive in terms of gate oxide integrity (GOI) and minority carrier lifetime (MCLT) in prefurnace wet processes. The presence of metallic impurities in wet chemicals such as hydrogen peroxide degrades GOI and MCLT when the last cleanup process involves RCA cleaning chemicals. However, HF-last process introduces a highly hydrophobic and reactive surface created by HF etching of oxide on the wafer. This HF-etched surface leaves defects called "water marks" after the drying process.[7] Water marks created before the gate oxidation can cause electrical failure due to locally thicker oxide formation. In this paper, in-line observation and classification of water marks after drying is presented with the experimental understanding of causes of these water marks in terms of wettability of wafer and drying methods.

## Experimental

The samples used were 6 in. (150 mm) p(100) wafers with 0.8 Ω · cm resistivities with and without patterns on them. Patterns were made on bare silicon and oxide-coated wafers to have hydrophilic and hydrophobic surfaces. Wafers were cleaned with ozonated piranha ($H_2SO_4 + O_3$) at 130°C for 20 min and followed by SC1 (1:2:10, $NH_4OH$:$H_2O_2$:$H_2O$) cleanup at 80°C for 10 min. Then wafers with and without pattern were etched in 0.5 weight percent (w/o) HF for 75-1100 s to obtain surfaces with different wettabilities, *i.e.,* hydrophilic, hydrophobic, or mixture of both surfaces. Hydrophilic wafers were prepared both by thermal oxidation and RCA wet chemical processes. The heterogeneous wafers having both hydrophobic and -philic sites were prepared by growing two different thicknesses of oxide film and etching them in HF to strip off the thin oxide

* Electrochemical Society Active Member.